



**Structural and Electrochemical Properties of NASICON-
 $\text{Na}_3\text{Cr}_y\text{Fe}_{(2-y)}(\text{PO}_4)_3$ Cathodes for Na-ion Batteries**

A Thesis

Submitted in partial fulfilment for the degree of

Master of Science (M. S.)

As a part of Integrated-PhD program (Chemical Science)

By

Mr. Mohd Arif



J N C A S R

New Chemistry Unit (NCU)

Jawaharlal Nehru Centre for Advanced Scientific Research

(An Institution Deemed to be University)

Bengaluru-560064 (India)

March-2022

**Dedicated to my beloved
family**

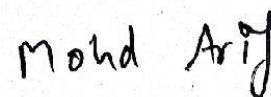
DECLARATION

I hereby declare that the content in this thesis entitled as "**Structural and Electrochemical Properties of NASICON- $\text{Na}_3\text{Cr}_y\text{Fe}_{(2-y)}(\text{PO}_4)_3$ Cathodes for Na-ion Batteries**" is the result of investigations carried out by me at the ENERGY STORAGE & CONVERSION LABORATORY, New Chemistry Unit (NCU), Jawaharlal Nehru Centre for Advanced Scientific Research, Bengaluru, India under the supervision of Dr. Premkumar Senguttuvan and that it is not submitted elsewhere for the award of any degree or diploma.

In keeping with the general practice in reporting the scientific observations, due acknowledgement has been made whenever the work described is based on the findings of other investigators. Any omission that might have occurred due to oversight or error in judgement is regretted.

Date: 11th April 2022
Bengaluru, India

Mohd Arif



CERTIFICATE

I hereby declare that the content in this thesis entitled as " **Structural and Electrochemical Properties of NASICON- $\text{Na}_3\text{Cr}_y\text{Fe}_{(2-y)}(\text{PO}_4)_3$ Cathodes for Na-ion Batteries** " has been carried out by **Mr. Mohd Arif** at the New Chemistry Unit (NCU), Jawaharlal Nehru Centre for Advanced Scientific Research, Bengaluru, India under my supervision and that it is not submitted elsewhere for the award of any degree or diploma.



Date: 11th April 2022

Dr. Premkumar Senguttuvan

Bengaluru, India

(Research Supervisor)

Acknowledgements

I thank to my supervisor Dr. Premkumar Senguttuvan for his guidance, support and encouragements to understand recent advancement and explore science.

I thank to Prof. C.N.R Rao, F.R.S., for being the constant source of inspiration for me. I admire him for his enthusiastic outlook for science.

I thank to Prof. Eswaramoorthy Muthusamy for his guidance, support and encouragements during my hard time.

I am also thankful to all faculty members of New Chemistry Unit, Chemistry and Physics of Materials Unit for giving me opportunity to nurture in science.

I thank to my course instructors Prof. M. Eswaramoorthy, Prof. S. Rajaram, Prof. P. Senguttuvan, Prof. R. Viswanatha, Prof. B. K. Sarma, Prof. J. Haldar, Prof. S. Agasti, Prof. A. Sundaresan, Prof. T. K. Maji, Prof. B. Saha. Prof. S. Balasubramanian, Prof. S. J. George, K. Bisvas, Prof. S. C. Peter for their excellent course work.

I am thankful to all my past and present labmates, Ms. Suchi Smita Biswas, Mr. Abhishek, Ms. Nijita, Ms. Divya, Ms. Soumita, Mr. Bhaskar, Mr. Biplab, Mr. Aridham, Mr, Subham, Mr. Amit, Ms. Vinita, Mrs. Radha.

I am thankful to all friends and classmates, Mr Amit, Mr. Rahul, Mr. Surya, Mr. Hariharan, Mr. Devesh, Mr. Suhas, Ms. Dipanjana, Mr Aashish, Mr. Uttam, Mr. Anustup, Mr. Vinay, Mr. Animesh, Mr. Tarak, Mr. Aditya, Ms. Alice, Ms. Sohini, Ms. Surabhi, Ms. Swarnima, Ms. Deeskha, Ms. Ankita, Ms. Yashwini who make my life unjoyful at JNCASR.

I thanks to all my past and present friends.

I am also thankful to Mrs. Melissa and Mr. Naveen (NCU), Mr. Vasu, Mrs. Meenakshi, Mrs. Usha ma'am, Mr. Anil for XRD, all mesh staff, Dhanvantri for keeping my health at upmost, Mr. Ruther Lewis for providing me DSC data on time and all JNCASR community.

Finally, and most importantly, my parents, sisters, and brothers who are always there with me without any conditions. I am fortunate to have them in my life.

LIST OF ABBREVIATIONS

XRD	X-ray Diffraction.....
PXRD	Powder X-ray Diffraction.....
FESEM	Field Emission Scanning Electron Microscopy.....
DSC	Differential Scanning Calorimetry.....
NASICON	Sodium (Na) Super (S) Ionic (I) Conductor (CON).....

CONTENTS:

DECLARATION.....	(i)
CERTIFICATE.....	(ii)
ACKNOWLEDGEMENTS.....	(iii)-(iv)
LIST OF ABBREVIATIONS.....	(vi)
CONTENTS.....	(vii)-(viii)

Chapter 1: Introduction to Batteries

1.1. Introduction.....	1-3
1.2. The working principle of Na-ion batteries.....	4
1.3. General Concepts and a Few Techniques Used.....	5-9
1.3.1. Galvanostatic Cycling with Potentials Limitation.....	5
1.3.2. Rietveld Refinement.....	5
1.3.2.1. Rietveld discrepancy value: R factor and goodness-of-fit χ^2 ..	5
1.3.2.2. Weighted profile R-factor (Rwp).....	6
1.3.2.2.1. Expected R-factor (R _{exp}).....	6
1.3.2.2.2. Goodness-of-fit χ^2	6
1.3.4. Solid-Electrolytes-Interphase (SEI)	7
1.3.5. Coulombic Efficiency.....	7
1.3.6. Gibb's Free Energy (ΔG)	8
1.3.7. Open Circuit Voltage (V_{oc})	9
1.3.8. C-Rate.....	9

1.4. Classification of Batteries.....	9-10
1.4.1. Primary Batteries.....	9
1.4.2. Secondary Batteries.....	10
1.5. Components of Secondary Battery.....	11-15
1.5.1. Anode Materials.....	11
1.5.2. Cathode Materials and their Classifications.....	12-15
1.5.2.1. Layered Oxides.....	12
1.5.2.2. Spinel Oxides.....	13
1.5.2.3. Polyanionic Oxides.....	13
1.5.3. Electrolytes.....	15
1.6. References.....	16-18

Chapter 2: Structural and Electrochemical Properties of NASICON- $\text{Na}_3\text{Cr}_y\text{Fe}_{(2-y)}(\text{PO}_4)_3$ Cathodes for Na-ion Batteries

2.1. Introduction.....	19-21
2.2. Experimental Section.....	21-23
2.2.1. Chemicals.....	21
2.2.2. Synthesis.....	21-22
2.2.3. Characterization.....	23
2.3. Results and Discussion.....	24-30
2.4. Conclusion.....	31
2.5. References.....	32-33

Chapter 1: Introduction to Batteries

1.1. Introduction

As we know, the world population is growing; the world population in 2015 was 7.2 billion. Nevertheless, now it increased in 2022 to 7.7 billion.¹ Consequently, the revolution in industries because of significant changes in living standards for the general population. Moreover, rapid development in the fields of chemical manufacturing, textile factories, and automobile engineering.^{2,3} However, it led to the abrupt change in the environment climate and created severe public health issues, like several types of disease even death.⁴ The newton's third law comes into play, stating that "to every action, there is an equal and opposite reaction." The research from World Health Organization (WHO) and United Nations Development Program (UNDP) concluded that global warming is due to human activities.⁵ Rapid industrialization heavily depends upon fossil-fuels-based energy like coal, oil, and natural gas. Thus, led to the emission of greenhouse gases, such as CO₂ and particulate, leading to dense fogs and air pollution. It is estimated that CO₂ emission from only fossil-fuels in 1960 was 9.39 billion tons; however, it is increased to 34.8 billion tons in 2020.⁶ Consequently, it increases the average earth's temperature following the melting of the glacier. Therefore, it needs rigorous research for an alternative source of green energy, like solar⁷ and winds energy.⁸ Nevertheless, the challenge is the transportation and storage of these forms of energy. Hence, electrochemical energy storage is one of the viable choices, such as capacitors⁹, batteries¹⁰, and fuel-cell¹¹ can partially solve such an issue (Fig. 1.2). We can see an increment of the CO₂ in billion tons vs year, 1750 to 1850 there is almost no emission of CO₂, 1850 to 1950 there is less emission of CO₂. However, from 1950 to 2020, there is drastically emission of CO₂, according to data from the Global Carbon Project (Fig. 1.1).¹² Rechargeable secondary batteries for electrochemical energy storage are the most efficient and leading technology available in today's market.¹³

A rechargeable battery is a pertinent electrochemical device that converts chemical energy into electricity and vice-versa. The lithium-ion batteries (LIBs) technology played a highly essential role and therefore matured in the market for portable electronic devices and electric vehicles.¹⁴ Fig.1.2 shows the Ragone plot of the various electrochemical system: batteries have higher energy density than capacitors.¹⁵

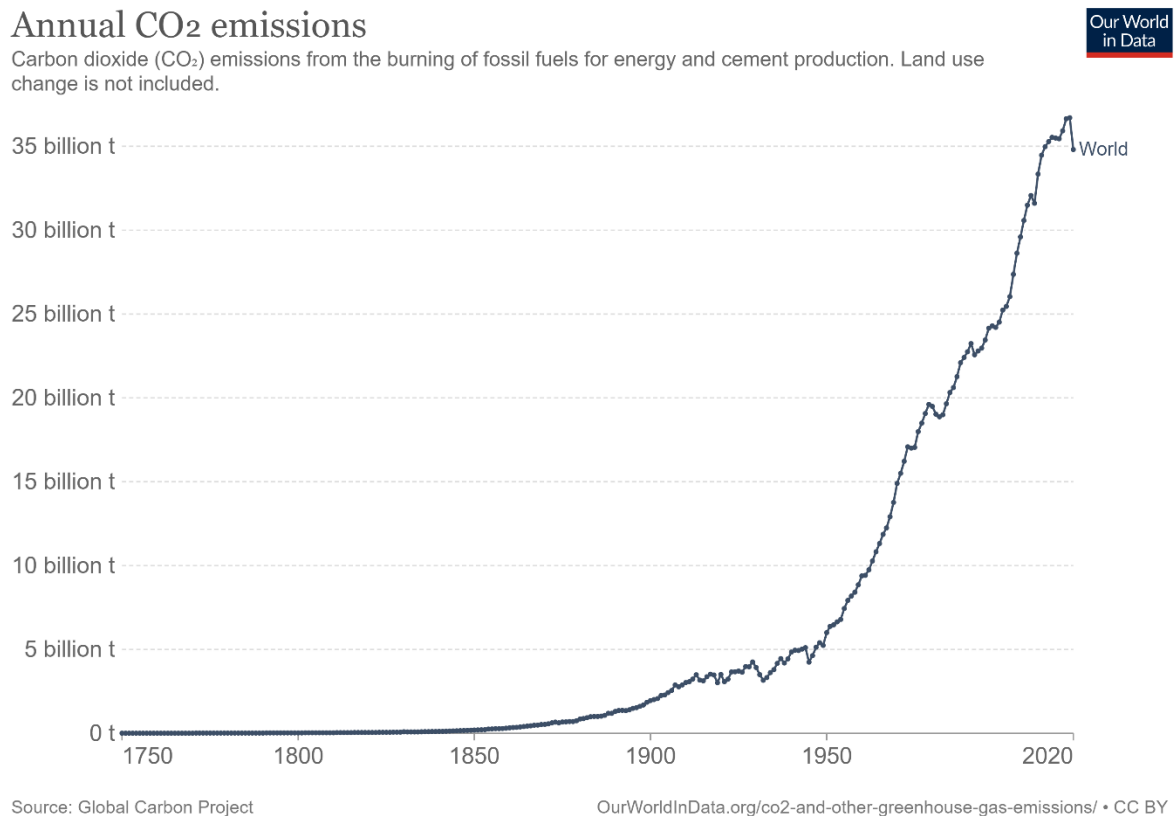


Figure 1.1. The plot of annual CO₂ emissions from burning fossil fuels and cement production Reproduce from reference,⁶ 2020 Global Energy Project.

Therefore, lithium-ion batteries technology has the potential that can be used for grid energy applications. however, the implementation of LIBs technology is limited because of the high cost and availability of lithium metal.¹⁶ Hence, the situation demands for batteries technology with similar chemistry but high in abundance and low in cost. Presently, sodium-ion batteries (SIBs) are emerging as Na is high in abundance and low in cost as compared to lithium metal (Figure 1.3).

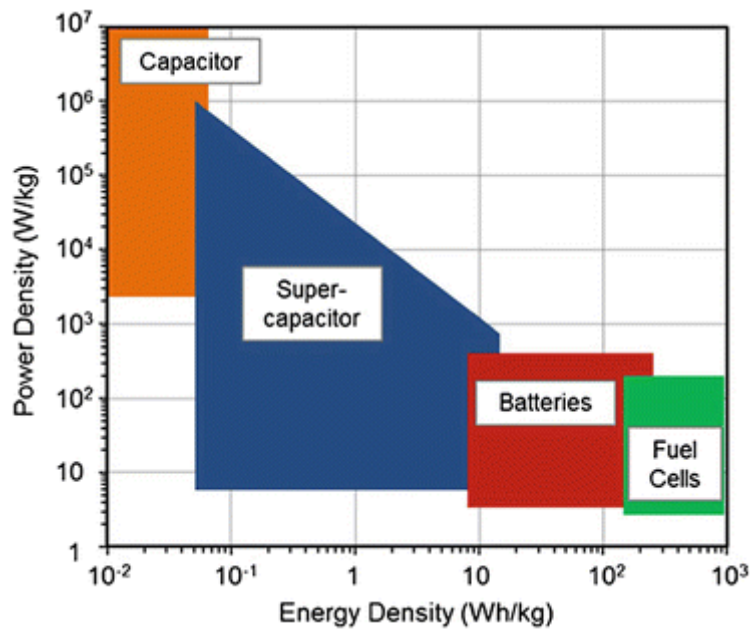


Figure 1.2. Ragone plot of the various electrochemical system. Reproduce from reference,¹⁵ 2019 Springer.

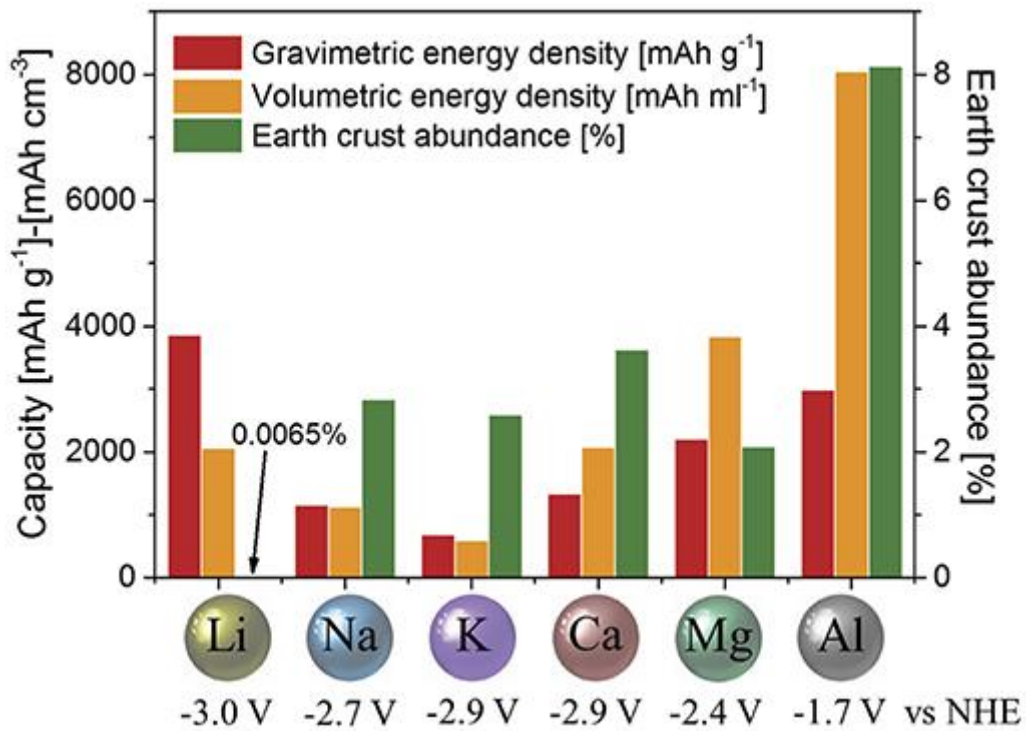


Figure 1.3. A plot of capacity, Earth abundance vs. reduction potentials (vs. NHE) of different metal elements. Reproduce from reference,¹⁷ 2016 Advanced Materials.

1.2. The working principle of Na-ion batteries

The schematic and operational principles of SIBs are analogous to LIBs. Figure 1.4 shows a schematic diagram of fundamental parts of and working principle of LIBs.

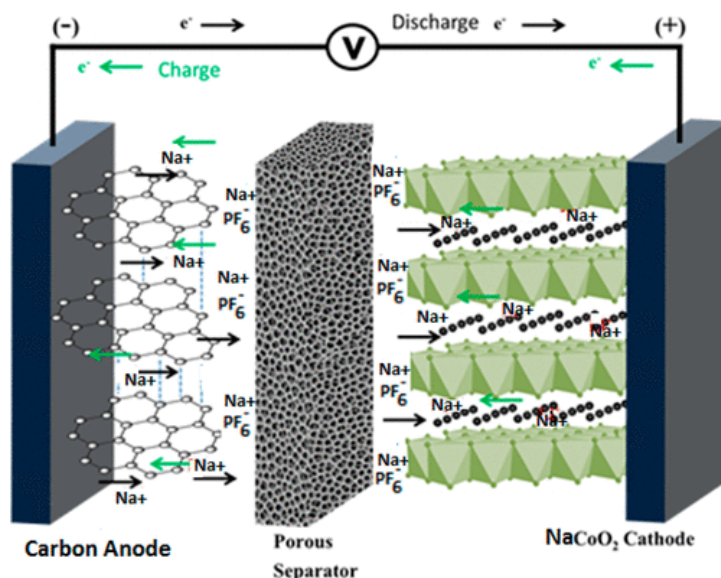


Figure 1.4. The schematic of a sodium-ion battery. Reproduce from reference,¹⁶ 2020 ACS energy letters.

It consists of three major parts: anode, cathode, and electrolyte. The cathode and anode are separated by a separator soaked with electrolytes which may be liquid (salts are dissolved in solvent: aqueous or organic). In SIB, sodium salts are dissolved in non-aqueous solvents. Moreover, it may be solid polymers,¹⁸ gel polymers, or ceramic electrolytes.¹⁹ The current collector is used to collect and distribute the electrons throughout the electrodes. In SIBs, sodium ions move from anode to cathode in the electrolytes through the porous media during discharge, and electrons travel from anode to cathode through the external circuit to balance the charge. As a result, the cathode gets reduced, and shuttling ions get inserted into the cathode materials. Additionally, during charging, electrons and ions move in a reverse direction. The electrochemical reaction happening in the batteries are the bulk phenomena rather than surface phenomena as taking place in the capacitors and supercapacitors.¹⁵

1.3. General Concepts and a Few Techniques Used

1.3.1 Galvanostatic Cycling with potential Limitation (GCPL)

GCPL is a chrono-potentiometric technique in which constant current (i) is applied to the working electrode, i.e., cathode, and its potential is measured as a function of time.²⁰ By the convention of batteries, its current sign is positive during charging and negative during discharging. Using the GCPL technique, the electrode materials' specific cell capacity and stability can be assessed upon cycling. Moreover, it gives us additional information about the presence of any irreversible redox process like SEI formation and electrolytes decomposition. Additionally, we can also assess the difference in the coulombic efficiency from this technique.

1.3.2. Rietveld²¹ refinement

It is a refinement technique used to fit a known structure model to the experimentally measured data by simulating the data profile. The height, weight, and position of the reflected powder X-ray diffraction (PXRD) patterns can be used to determine the many aspects of materials structure. If the applied model is correct, it will predict the "true" intensity values. This technique is more commonly used for PXRD. It includes the non-linear least-squares method after giving a valid initial approximation of many free parameters, like peak shapes, unit cell dimensions, and coordinates of all atoms in the crystal structure. We can assess other parameters from this information while still being reasonably refined.

Moreover, Hugo Rietveld first described it in 1969 to refine crystalline materials. Presently, many software, like FULLPROF²² and GSAS,²³ have been developed, incorporating many parameters for a better fit. The parameters defined in the fitting include peak position, peak shapes, atomic coordinate, and its occupancy, addition of different phases, background, etc.

1.3.2.1. Rietveld discrepancy value: R factor and goodness-of-fit χ^2 :

R factor: It is mainly classified into two types: **Weighted profile R-factor** labeled as **Rwp** and **Expected R-factor** labeled as **Rexp**.

1.3.2.2. Weighted profile R-factor (Rwp):

Suppose the intensity value simulated from a model will be represented as $Y_{c,i}$ where **C** is defined as calculated from the model. Moreover, observe intensity is labeled as a $Y_{o,i}$ where **o** represents the observed value, and **i** is defined as an intensity measure at 2θ value $2\theta_i$. The Rietveld technique optimizes the model function to minimize the weighted sum of the squared difference between the observed and calculated values, i.e., to minimize $\sum [W_i (Y_{o,i} - Y_{c,i})^2]$.

The weighted is represented as W_i , which is $1/\sigma^2[Y_{o,i}]$, where $Y_{o,i}$ represents **uncertainty estimates**.

The weighted profile R-factor Rwp is given as;

$$R_{wp} = \frac{\sum [W_i (Y_{o,i} - Y_{c,i})^2]}{\sum W_i (Y_{o,i})^2}$$

1.3.2.2.1. Expected R-factor (Rexp): If the model is ideal and accurately predicts the true value for each $Y_{o,i}$ value, then the average value of $(Y_{o,i} - Y_{c,i})^2$, will be equal to $\sigma^2[Y_{o,i}]$ and expected value of $W_i (Y_{o,i} - Y_{c,i})^2$ equal to one. If the one obtained from this ideal model would be the best possible value, the $\sigma [Y_{o,i}]$ values are correct. This "**best possible Rexp**" value is the highest use of the full concept and is called the expected R-factor, which is given bellow;

$$(R_{exp})^2 = N / \sum W_i (Y_{o,i})^2$$

Where N is called several data points.

1.3.2.2.2. Goodness-of-fit χ^2

Let the model be ideal, and the uncertainty estimate value is correct, then considering the expected value $(Y_o, i - Y_c, i)^2 / \sigma^2[Y_o, i]$ will be one. The value of "Chi" can never be less than one if it happens there could be one of the two things is true: (1) "The estimated uncertainty for the data must be overestimated or (2), so many parameters have been introduced that the model is adjusting to fit the noise".²⁴

1.3.4. Solid-Electrolytes-Interphase (SEI)

This is a passivation layer formed on the lithium/sodium metal anode upon cycling due to the decomposition of the electrolytes. The lithium/sodium metal is highly reactive and reacts with organic electrolytes, consisting of solvents in which salts were dissolved and added additive. Additionally, dense and intact SEI formed restricts the tunnelling of the electrons and thus further reduction of the electrolytes. Therefore, it is substantial for a battery's chemical and electrochemical stability. In addition, formed SEI led to capacity fading, poor power density, and increasing battery resistances. The formation of the SEI occurs when the Electrode's redox potential in batteries lies outside the electrolytes' electrochemical window.²⁵ In more specific ways, the electrochemical potential lies above the Lowest Unoccupied Molecular Orbital (LUMO) and below the Highest Occupied Molecular Orbital (HOMO). Fig. 1.5 shows the energy diagram of the electrolytes and the electrochemical potential of the electrodes (anode and cathode).

1.3.5. Coulombic Efficiency

Efficiency is the crucial parameter of the secondary battery systems. The released capacity of batteries is always less than its charging capacity. In other words, discharging capacity is always less than charging capacity. It can be described as a ratio between the amount of Li^+ ions or electrons returning to the cathode and the amount of Li^+ ions or electrons departing from the cathode in a full cycle.²⁶ It is expressed as an equation given (page 8),

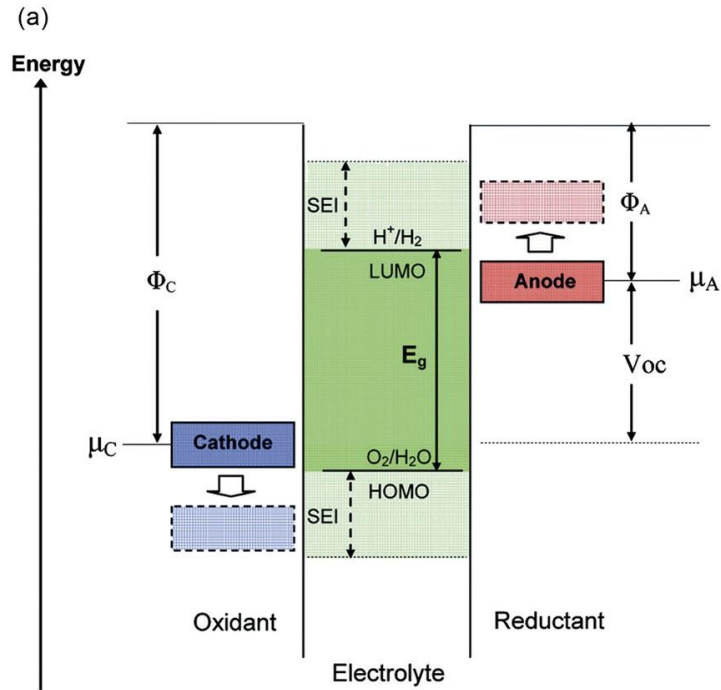


Figure 1.5. Schematic Open-circuit energy diagram of the electrolytes. Reproduce from reference,²⁵ 2018 (npj) Nature.

$$\begin{aligned}
 \text{Efficiency} &= \frac{\text{Discharge Capacity}}{\text{Charge Capacity}} \\
 &= \frac{\text{Total number of Li}^+ \text{ ions back to cathode}}{\text{Total number of Li}^+ \text{ ions departing from cathode}} \\
 &= \frac{\text{Total number of electrons back to cathode}}{\text{Total number of electrons departing from cathode}}
 \end{aligned}$$

1.3.6. Gibb's Free Energy (ΔG)

It determines the feasibility of the reactions. From a thermodynamic point of view, it is a useful work obtainable from a thermodynamic system at constant temperature and constant pressure.²⁷

The difference in Gibbs free energy (ΔG) for the reaction between the charged and discharged state is given by the equation:

$$\Delta G = \Delta H_r - T\Delta S_r = \Delta U_r + P\Delta V_r - T\Delta S_r$$

Where T is the temperature, P is the pressure of the system, and the terms $P\Delta V_r$, $T\Delta S_r$ correspond to changes in the volume and entropy of the system.

1.3.7. Open Circuit Voltage (V_{oc})

Open circuit voltage is determined by the difference between chemical potential of the anode (μ_A) and the cathode (μ_C) of the cell. It is also termed as a working voltage, which is given by equation:²⁸

$$V_{OC} = \frac{\mu_A - \mu_C}{e}$$

Where e is the magnitude of the electronic charge.

1.3.8. C-Rate

It measures the rate of cycling of a battery, which means the rate at which charge and discharge is happening. In other words, C is a current per unit capacity. Moreover, C -rate represents the current rate rather than the current density.²⁹ Let's C -rate is $C/10$ which means it will take 10h to reach its maximum current.

1.4. Classification of Batteries:

Batteries are generally classified into two types

1.4.1. Primary Batteries

1.4.2. Secondary batteries

1.4.1. Primary Batteries:

Primary batteries are the combination of non-rechargeable cells-a galvanic cell, i.e., It is used once after charge, in which chemical energy is stored during charging and converted into electric energy during discharging. In general, the electrochemical reaction occurring in the cell is not reversible. The components of the cell are given on page 10 (Figure 1.6).

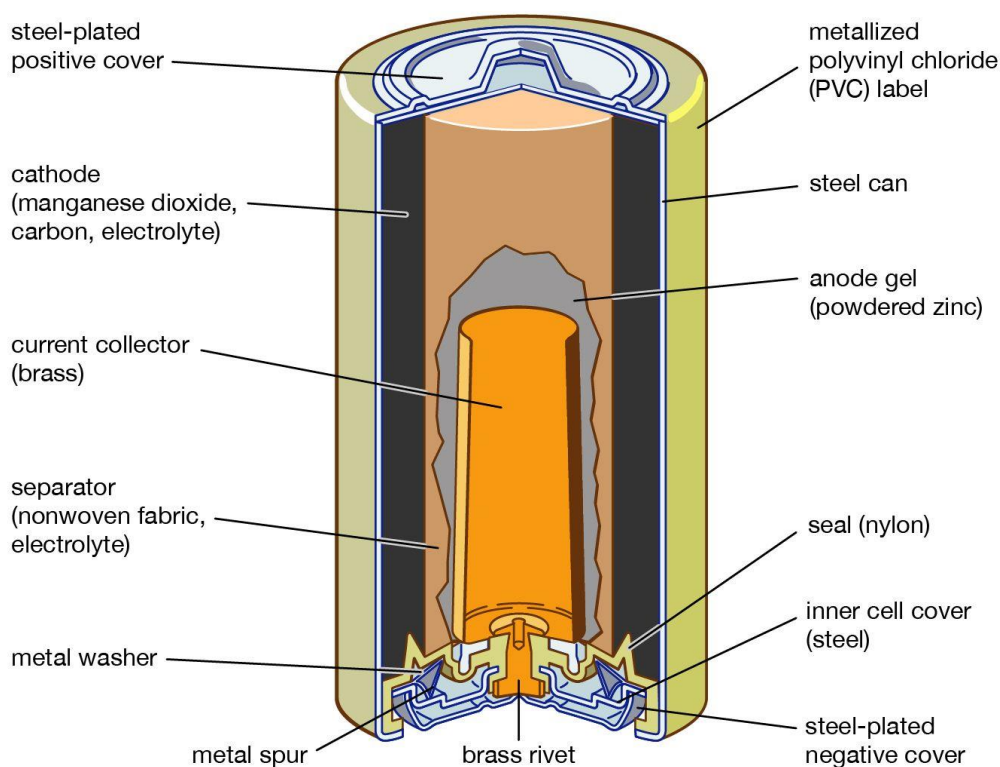


Fig. 1.6. Schematic representation of the components of a primary cell. Reproduce from reference,³⁰ 2021 encyclopaedia Britannica.

1.4.2. Secondary Batteries:

The secondary batteries are a combination of rechargeable cells. It consists of primarily three components: Anode, Cathode, and Electrolyte, that participate in electrochemical energy storage. In secondary batteries, during discharging, ions (Li in case of Li-ion battery and Na in case of Na-ion battery, etc.) move from anode to cathode through porous media and vice versa during charging. In addition, salts ion is dissolved in the solvents. The secondary battery cell (Na-ion cell) schematic representation is given on page 11 (Figure 1.7).

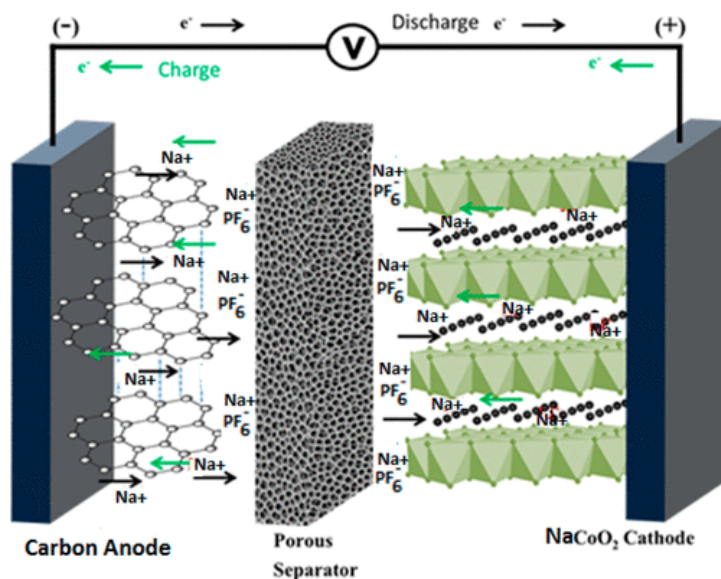


Fig. 1.7. Schematic representation of secondary battery cell. Reproduce from reference,¹⁶ 2020 ACS energy letter.

1.5. Components of secondary Battery:

1.5.1. Anode Materials

An anode is a negative electrode in rechargeable batteries. Good anode material for practical applications is expected to have a high capacity, low potential, long cycle life, and high safety. The lithium-metal anode was used in lithium-ion batteries because of its low electrode potential and high energy density. However, Li-metal suffers from safety, dendrite growth on the anode due to electrolyte degradation, and formation of solid electrolytes interphase (SEI). In addition, SEI on anode impedes the ion's transportation to the anode. Therefore, an alternative of lithium metal has been used to get rid of safety concerns such as $\text{Li}_4\text{Ti}_5\text{O}_{12}$, graphite, and Silicon.³¹ In the case of silicon with cycling, Li-metal intercalates/de-intercalate resulting in a considerable volume change (>300%) in comparison to graphite anode.³² This significant volume change causes several issues in the Si anode, such as cracking, fracture, disintegration, electric isolation of the Si materials and the current collector. Although, the specific capacity of Si anode is ten times higher than conventional graphite anode (372 mAh/g).

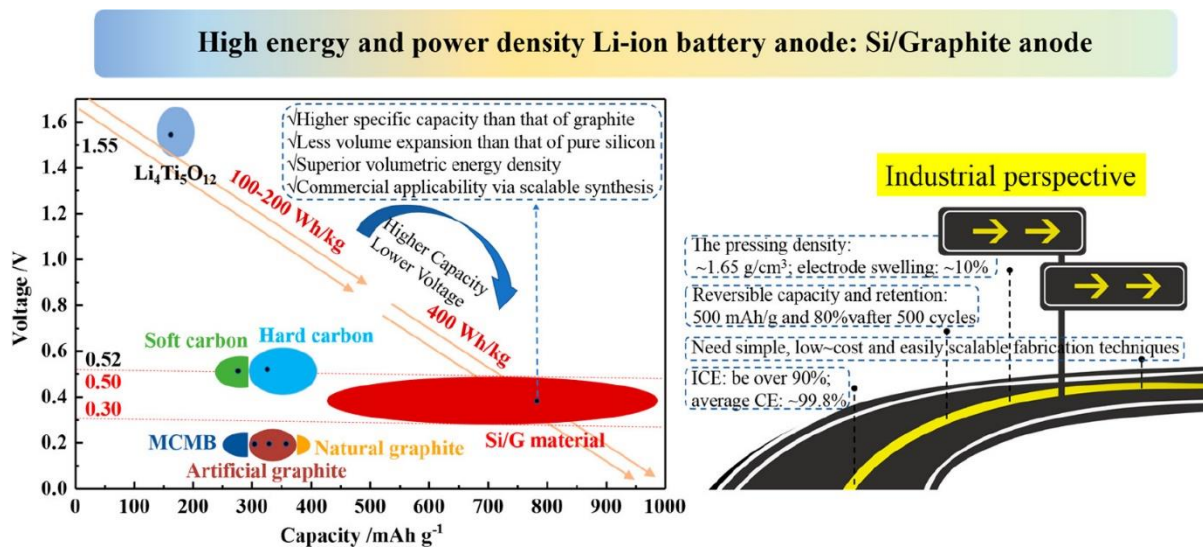


Fig. 1.8. Schematic representation of voltage vs. capacity of silicon (Si)/graphite and other commercial anode materials. Reproduce from reference,³² 2021 ACS energy fuels.

1.5.2. Cathode Materials and their classifications

There have been several types of cathode materials commercialized for Li-ion batteries under considerable research efforts. In addition, electrochemical energy storage materials are the critical factor in determining the performances, such as capacity, lifespan, and safety. The cathode materials are broadly classified as: layer oxides, spinel oxides, polyanion oxides, Prussian Blue Analogues (PBAs), etc. Here, I have briefly outlined the first three cathode materials.

1.5.2.1. Layered Oxides

The very first cathode materials for Li-ion batteries come into the market is LiCoO_2 . Layered oxide materials, discovered by Chemistry Nobel Laureate, Prof. J. B. Goodenough^{33,34} Moreover, it is still widely being used for communication, computers, and consumer electronics. It displays high theoretical specific as well as volumetric capacity, 274 mAh/g, and 1363 mAh/cm³, respectively. The layer crystal structure of LiCoO_2 is represented in Fig. 1.9.

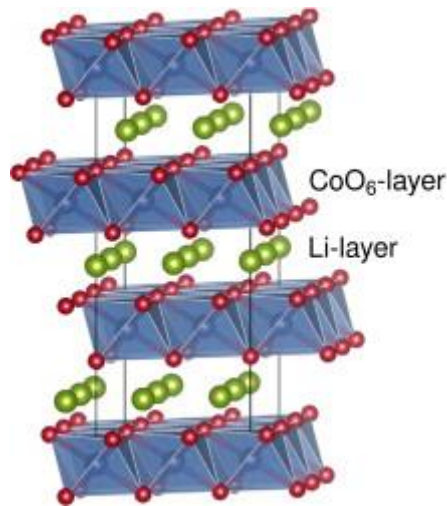


Figure 1.9. Schematic representation of LiCoO_2 layer crystal structure. Reproduce from reference,³³ 2015 Energy Mat Adv.

1.5.2.2. Spinel Oxides

The spinel oxides have a three-dimensional (3D) crystal structure. Moreover, it has good 3D crystal structure stability along with high ionic and electronic conductivity. One of the most famous spinel oxides for the cathode materials is LiMn_2O_4 , which Prof. Goodenough's research group proposed it in 1984. The practical and theoretical specific capacities of LiMn_2O_4 are 120 mAh/g and 148 mAh/g, respectively.³⁵ Fig. 1.10. Shows 3D crystal structure of LiMn_2O_4 , Mn octahedrally surrounded by six oxygen atoms and link through edge-sharing another octahedron offer 3D lithium-ion diffusion pathway as we can see in Fig. 1.10 (b).

1.5.2.3. Polyanion Oxides

Coming to the third class of cathode materials, polyanion oxides, a part of Manthiram's PhD. Dissertation work in India. He has synthesized $\text{Fe}_2(\text{MoO}_4)_3$ and $\text{Fe}_2(\text{WO}_4)_3$ for the hydrogen reduction,³⁶ which crystallizes in the NASICON-related framework structure. Similarly, other materials have been proposed, like $\text{Fe}_2(\text{SO}_4)_3$; in general, it can be represented as $\text{Fe}_2(\text{XO}_4)_3$ where X could be Mo, W, P, and S. The crystal structure of the NASICON-related framework represented in Fig.1.11.

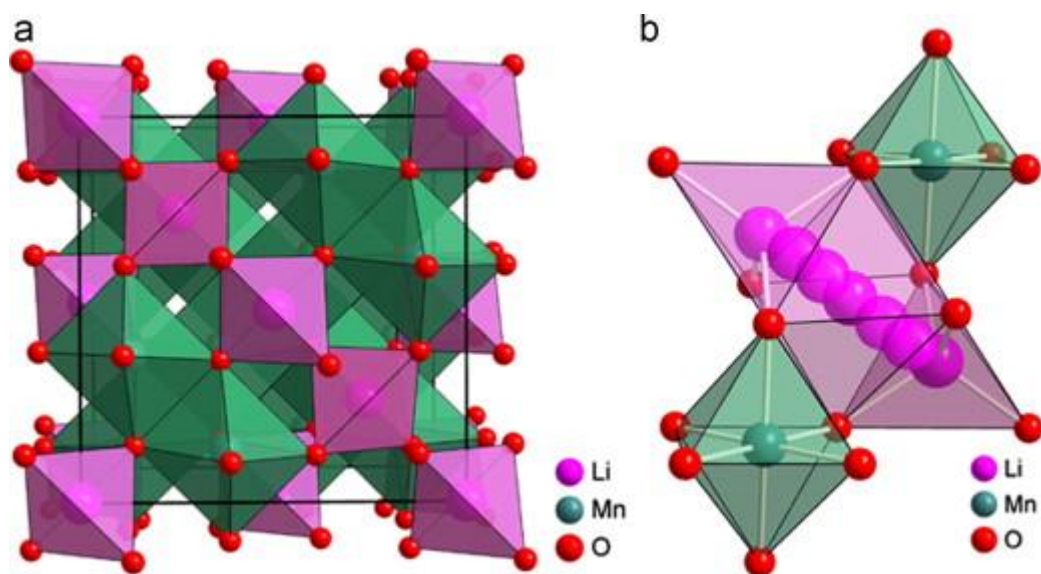


Figure 1.10. (a) the 3D crystal structure of LiMn_2O_4 (b) its corresponding Li-ion diffusion pathways. Reproduce reference,³⁵ 2013 Elsevier.

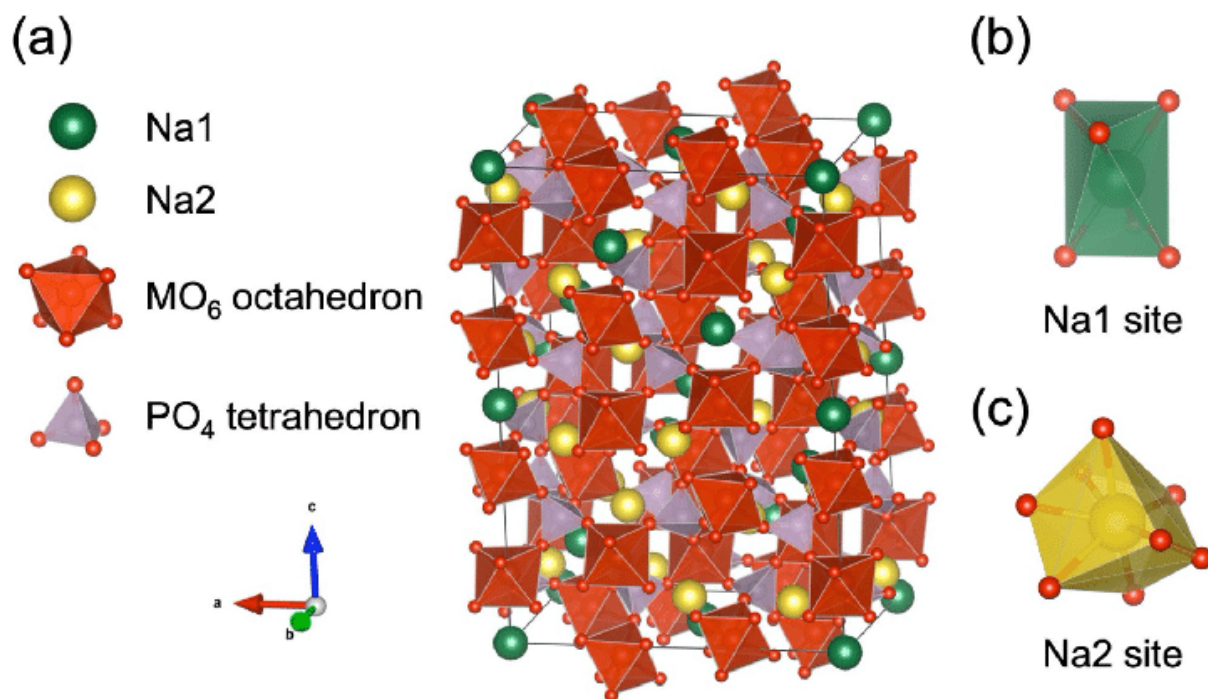
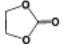
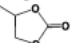
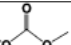
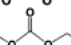
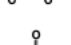


Figure 1.11. The crystal structure of the NASICON-type framework. Reproduce from reference,³⁷ 2020 Electrochemical Soc. of Japan.

1.5.3. Electrolytes

The electrolytes are one of the main components of the batteries physically sandwiched between two electrodes, namely, the cathode and the anode. The job of the electrolytes is to transport the ions between the electrodes of the rechargeable batteries. The suitable electrolytes for lithium/sodium-ion batteries are non-aqueous and aprotic liquid electrolytes. Considering the cyclic propylene carbonate (PC), ethylene carbonate (EC) has high dielectric constant and high viscosity. The high viscosity of EC and PC makes it low transportable to ions. Moreover, diethylene carbonate (DEC), dimethyl carbonate (DMC), and ethyl methyl carbonate (EMC) have low dielectric constant and low viscosity. Hence, it is used as an additive in the electrolytes. Additionally, Na/LiClO₄ and Na/LiPF₆ are generally used to source Li/Na ions. Table 1 listed a few solvents and corresponded their properties.³⁸

Table 1. Organic Carbonates and Esters as Electrolyte Solvents

Solvent	Structure	M. Wt	T _m / °C	T _b / °C	η/cP 25 °C	ε 25 °C	Dipole Moment/debye	T _f / °C	d/gcm ⁻³ , 25 °C
EC		88	36.4	248	1.90, (40 °C)	89.78	4.61	160	1.321
PC		102	-48.8	242	2.53	64.92	4.81	132	1.200
DMC		90	4.6	91	0.59 (20 °C)	3.107	0.76	18	1.063
DEC		118	-74.3 ^a	126	0.75	2.805	0.96	31	0.969
EMC		104	-53	110	0.65	2.958	0.89		1.006

1.6. References

- (1) Bureau, U. sensus. World Population Review. 2022 World Population by Country. Retrieved Mar 7, 2022, from <https://worldpopulationreview.com/>.
- (2) Teker, S.; Koc, T. C. Industrial Revolutions and Its Effects on Quality of Life. *PressAcademia* **2019**, *9* (9), 304–311. <https://doi.org/10.17261/pressacademia.2019.1109>.
- (3) Violeta Sima 1,* , Ileana Georgiana Gheorghe 1, J. S. 2 and D. N. 3; 1. Influences of the Industry 4.0 Revolution on the Human Capital Development and Consumer Behavior: A Systematic Review. *Sustainability* **2020**, *12*, 4035–4063. <https://doi.org/10.1007/s12652-021-03177-x>.
- (4) Ravishankara, A. R.; Rudich, Y.; Pyle, J. A. Role of Chemistry in Earth’s Climate. *Chemical Reviews*. American Chemical Society May 27, 2015, pp 3679–3681. <https://doi.org/10.1021/acs.chemrev.5b00226>.
- (5) NASA. <https://climate.nasa.gov/resources/global-warming-vs-climate-change>.
- (6) Hannah Ritchie and Max Roser (2020) - “CO₂ and Greenhouse Gas Emissions”. Published online at OurWorldInData.org. Retrieved from: ‘<https://ourworldindata.org/co2-and-other-greenhouse-gas-emissions>’ [Online Resource].
- (7) Philosophy, L.; Ma, U.; Sari, A. K.; Aziz, A.; Sari, A. K. DigitalCommons @ University of Nebraska - Lincoln A STUDY OF RENEWABLE ENERGY AND SOLAR PANEL LITERATURE THROUGH BIBLIOMETRIC POSITIONING DURING DigitalCommons @ University of Nebraska - Lincoln A STUDY OF RENEWABLE ENERGY AND SOLAR PANEL LITERATURE. *Libr. Philos. Pract.* **2021**, No. July, 1–17.
- (8) Thresher, R.; Robinson, M. Wind Energy Technology : Current Status and R & D Future. In *NREL*; 2008; pp 1–24.
- (9) Lukatskaya, M. R.; Bak, S.; Yu, X.; Yang, X.; Barsoum, M. W. Probing the Mechanism of High Capacitance in 2D Titanium Carbide Using In Situ X-Ray Absorption Spectroscopy. *Adv Energy Mat.* **2015**, 1–4. <https://doi.org/10.1002/aenm.201500589>.
- (10) Yu, X. Sodium-Sulfur Batteries with a Polymer- Coated NASICON-Type Sodium-Ion Solid Electrolyte Sodium-Sulfur Batteries with a Polymer-Coated NASICON-Type Sodium-Ion Solid Electrolyte. *Matter* **2019**, *1* (2), 439–451. <https://doi.org/10.1016/j.matt.2019.03.008>.
- (11) Fuel, B.; Performance, C.; Mesopores, A. C. Boosting Fuel Cell Performance With. *ACS Energy Lttter* **2018**, 8–11. <https://doi.org/10.1021/acsenerylett.8b00186>.
- (12) <https://ourworldindata.org/co2-emissions>.
- (13) Kim, S. Y.; Kundu, D.; Nazar, L. F. A 4 V Na + Intercalation Material in a New Na-Ion Cathode Family. *Adv Energy Mat* **2018**, *1701729*, 1–9. <https://doi.org/10.1002/aenm.201701729>.
- (14) Goodenough, J. B.; Park, K. The Li-Ion Rechargeable Battery : A Perspective. *Am Chem Soc* **2013**, 1–10.

- (15) Marichi, R. B. Efficient, Sustainable, and Clean Energy Storage in Supercapacitors Using Biomass-Derived Carbon Materials. *Springer Nat. Switz. AG* **2019**, 855–880.
- (16) Abraham, K. M. How Comparable Are Sodium-Ion Batteries To. *ACS Energy Lett.* **2020**, 3544–3547. <https://doi.org/10.1021/acseenergylett.0c02181>.
- (17) Elia, G. A.; Marquardt, K.; Hoepfner, K.; Fantini, S.; Lin, R.; Knipping, E.; Peters, W.; Drillet, J.; Passerini, S. An Overview and Future Perspectives of Aluminum Batteries. *Adv. Mater.* **2016**, *28*, 7564–7579. <https://doi.org/10.1002/adma.201601357>.
- (18) Yao, P.; Yu, H.; Ding, Z.; Liu, Y.; Lu, J.; Lavorgna, M. Review on Polymer-Based Composite Electrolytes for Lithium Batteries. *Front. Chem.* **2019**, *7* (August), 1–17. <https://doi.org/10.3389/fchem.2019.00522>.
- (19) Zhu, M.; Wu, J.; Wang, Y.; Song, M.; Long, L.; Siyal, S. H. Recent Advances in Gel Polymer Electrolyte for High-Performance Lithium Batteries. *J. Energy Chem.* **2019**, *37*, 126–142. <https://doi.org/10.1016/j.jechem.2018.12.013>.
- (20) EC-Lab – Application Note # 01 Protocols for Studying Intercalation Electrodes Materials : Part I : Galvanostatic Cycling with Potential Limitation (GCPL) I – Introduction EC-Lab – Application Note # 01 II – Galvanostatic Cycling with Potential Limitati. **2005**, 31–34.
- (21) Station, E. E. *A New Computer Program for Rietveld Analysis of X-Ray Powder Diffraction Patterns.*; 1981.
- (22) Rodríguez-carvajal, J.; Cea-cnrs, L. L. B. AN INTRODUCTION TO THE PROGRAM (Version July2001). 2001, p 139.
- (23) Dreele, A. C. L. & R. B. Von. *General Structure Analysis System (GSAS)* ,; 2004; Vol. 748.
- (24) Toby, B. H. R Factors in Rietveld Analysis: How Good Is Good Enough? *Powder Diffr.* **2006**, *21* (1), 67–70. <https://doi.org/10.1154/1.2179804>.
- (25) Wang, A.; Kadam, S.; Li, H.; Shi, S.; Qi, Y. Review on Modeling of the Anode Solid Electrolyte Interphase (SEI) for Lithium-Ion Batteries. *npj Comput. Mater.* **2018**, No. February. <https://doi.org/10.1038/s41524-018-0064-0>.
- (26) Xiao, J.; Li, Q.; Bi, Y.; Cai, M.; Dunn, B.; Glossmann, T.; Liu, J.; Osaka, T.; Sugiura, R.; Wu, B.; Yang, J.; Zhang, J.; Whittingham, M. S. Understanding and Applying Coulombic Efficiency in Lithium Metal Batteries. *Nat. Energy* **2020**, 1.8. <https://doi.org/10.1038/s41560-020-0648-z>.
- (27) Wikipedia, F. Gibbs Free Energy; 2011; pp 1–6.
- (28) Liu, C.; Neale, Z. G.; Cao, G. Understanding Electrochemical Potentials of Cathode Materials in Rechargeable Batteries. *Mater. Today* **2016**, *19* (2), 109–123. <https://doi.org/10.1016/j.mattod.2015.10.009>.
- (29) Society, T. E. The Chalkboard: C Rating of Batteries: A Misleading Concept, C Flux Rather than C Rate. *Electro. Chem. Soc.* **2018**, 1–3.
- (30) Schumm, Brooke. “battery”. Encyclopedia Britannica, 5 Mar. 2021, <https://www.britannica.com/technology/battery-electronics>. Accessed 7 March 2022.
- (31) Foix, D.; Franger, S.; Patoux, S.; Daniel, L.; Gonbeau, D. Electrode/Electrolyte

- Interface Reactivity in High-Voltage Spinel $\text{LiMn}_{1.6}\text{Ni}_{0.4}\text{O}_4/\text{Li}_4\text{Ti}_5\text{O}_{12}$ Lithium-Ion Battery. *J. Phys Chem* **2010**, 10999–11008.
- (32) He, S.; Huang, S.; Wang, S.; Mizota, I.; Liu, X.; Hou, X. Considering Critical Factors of Silicon / Graphite Anode Materials for Practical High-Energy Lithium-Ion Battery Applications. *ACS energy fuel* **2021**, 944–964. <https://doi.org/10.1021/acs.energyfuels.0c02948>.
- (33) Hausbrand, R.; Cherkashinin, G.; Ehrenberg, H.; Gröting, M.; Albe, K.; Hess, C.; Jaegermann, W. Fundamental Degradation Mechanisms of Layered Oxide Li-Ion Battery Cathode Materials : Methodology , Insights and Novel Approaches. *Mater. Sci. Eng. B* **2015**, 192, 3–25. <https://doi.org/10.1016/j.mseb.2014.11.014>.
- (34) Shen, X.; Zhang, X.; Ding, F.; Huang, J.; Xu, R.; Chen, X.; Yan, C.; Su, F.; Chen, C.; Liu, X.; Zhang, Q. Review Article Advanced Electrode Materials in Lithium Batteries : Retrospect and Prospect. *Energy Mat Adv* **2021**, 1–15.
- (35) Tianran, Z.; Daixin, L.; Tao, Z.; Jun, C. Understanding Electrode Materials of Rechargeable Lithium Batteries via DFT Calculations. *Prog. Nat. Sci. Mater. Int.* **2013**, 23 (3), 256–272. <https://doi.org/10.1016/j.pnsc.2013.04.005>.
- (36) Manthiram, A. A Reflection on Lithium-Ion Battery Cathode Chemistry. *Nat. Commun.* **2020**, 11 (1), 1–9. <https://doi.org/10.1038/s41467-020-15355-0>.
- (37) Ishado, Y.; Inoishi, A.; Okada, S. Exploring Factors Limiting Three-Na+Extraction from $\text{Na}_3\text{V}_2(\text{PO}_4)_3$. *Electrochemistry* **2020**, 88 (5), 457–462. <https://doi.org/10.5796/electrochemistry.20-00080>.
- (38) Xu, K. Nonaqueous Liquid Electrolytes for Lithium-Based Rechargeable Batteries. *Chem. Rev.* **2004**, 104 (10), 4303–4417. <https://doi.org/10.1021/cr030203g>.

CHAPTER 2

Structural and Electrochemical Properties of NASICON- $\text{Na}_3\text{Cr}_y\text{Fe}_{(2-y)}(\text{PO}_4)_3$ Cathodes for Na-ion Batteries.

2.1. Introduction

The demand for clean energy storage and conversion devices is overwhelmingly increasing to address the concerns over carbon footprint. Batteries are among the most delicate devices for energy storage because they have several advantages: high efficiency, easily portable, high energy, and power densities.^{1,2} Lithium-ion batteries (LIBs) are a mature and captured world market due to their high energy density, long cycle life, and low maintenances.^{3,4} Moreover, LIBs are gaining attention for electric vehicles and grid-scale applications.^{5,6} However, for grid-scale applications, cost, availability, and accessibility of lithium sources are open questions. On the contrary, sodium sources are abundant, inexpensive and easily accessible.^{7,8} Thus, potentially it can be used for large-scale applications.⁹

The materials chemistry and electrochemistry of Na-ion batteries are significantly different from the Li-ion batteries. Because, sodium has lower electrode potential than lithium (-2.71V vs. SHE of Na than -3.04V vs. SHE of Li) and lower energy densities.¹⁰ In addition, the cationic radius of sodium is larger than lithium (1.06 Å of Na^+ than 0.71Å of Li^+).¹⁰ Thus, it leads to the massive difference in intercalation chemistry of sodium and lithium, insertion potential, diffusion barrier, and stability of given hosts. Different cathode materials have been proposed for interaction/deintercalation (host) of sodium ions such as layered oxides,¹¹ polyanion oxides,¹² Prussian Blue Analogues (PBAs)¹³ etc. Although layered oxides deliver higher capacities (150-200 mAh g^{-1}), they suffer from multiple phase changes during charge/discharge or deintercalation/intercalation. The comparison of a half-cell of charge/discharge voltage versus specific capacity curve of $\text{Li}/\text{Li}_{1-x}\text{CoO}_2$ and $\text{Na}/\text{Na}_{1-x}\text{CoO}_2$ in Fig. 2.1. It shows stepwise

voltage profiles for sodium cells. They reflect the multiple phase changes of the NaCoO_2 crystal as Na^+ is deintercalated to form $\text{Na}_{1-x}\text{CoO}_2$ during charging vice versa during discharging. The crystal structure of both LiCoO_2 and NaCoO_2 is the same O3-type phase, consisting of CoO_2 slab and Na^+ or Li^+ are sandwiched between the slab along the c -axis of the $\text{A}_{1-x}\text{CoO}_2$ crystal (where $A = \text{Li}$ or Na).¹⁴ The crystal structure changes with the beginning removal of Na from the NaCoO_2 during the first charge. The CoO_6 form octahedra within which sodium ions in the O3-type phase are mainly stabilized at edge-shared octahedral sites. When Na^+ -ions are partially extracted during charging from the O3-type phase, the Na^+ -ions present at the prismatic sites become energetically stable and transform crystal to P3-phase. This is due to sliding CoO_2 slabs without breaking the Co-O bond. This transformation between octahedral to prismatic phase by sliding the slabs occurs in all the transition metal oxides used as a cathode material for Na-ion batteries.¹⁴ To sort out above bottleneck for Na-ion batteries, since it needs robust cathode materials (e.g., NASICON).^{5,15}

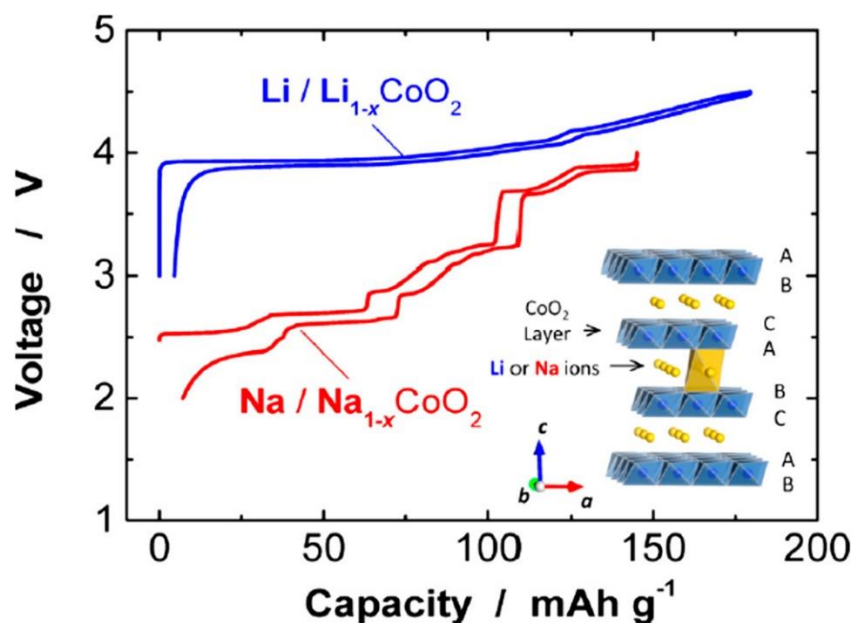


Figure 2.1 Schematic representation of voltage vs. capacity curves. Reproduce from reference,¹⁴ 2020 ACS energy letters.

NASICON phosphates are attractive class of materials as Na-ion cathodes due to their higher structural and thermal stabilities and faster Na-ion diffusivity. $\text{Na}_3\text{V}_2(\text{PO}_4)_3$ cathode delivers reversible capacities of $\sim 100 \text{ mAh g}^{-1}$ at an average voltage of 3.45 V vs. Na^+/Na^0 , corresponding to the activity of $\text{V}^{4+}/\text{V}^{3+}$ redox couple.¹⁵ Another NASICON cathode, $\text{Na}_3\text{Fe}_2(\text{PO}_4)_3$ is appealing because of earth-abundant iron precursor. It delivers stable capacities of $\sim 50 \text{ mAh g}^{-1}$ at 2.6 V vs. Na^+/Na^0 *via* concomitant reduction of Fe^{3+} to Fe^{2+} .^{16,17} Recently, NASICON- $\text{Na}_3\text{Cr}_2(\text{PO}_4)_3$ cathode has been reported for its high voltage redox activity ($\sim 4.5 \text{ V}$).¹⁸ However, it suffers from rapid capacity decay due to structural degradation happening at higher voltages.

In this work, we have tailored a series of NASICON- $\text{Na}_3\text{Cr}_y\text{Fe}_{(2-y)}(\text{PO}_4)_3$ ($y = 0, 0.5, 1, 1.5$ and 2) solution assisted solid-state synthesis. As the endmembers' (i.e., $\text{Na}_3\text{Cr}_2(\text{PO}_4)_3$ & $\text{Na}_3\text{Fe}_2(\text{PO}_4)_3$) redox activities are limited to maximum of one Na exchange per formula unit (i.e., equivalent to 50 mAh g^{-1}). Here, we attempted to utilize two redox couples $\text{Cr}^{4+}/\text{Cr}^{3+}$ and $\text{Fe}^{3+}/\text{Fe}^{2+}$ in this NASICON host in order to realize higher storage capacities.

2.2. Experimental Section

2.2.1. Chemicals

$\text{Cr}(\text{NO}_4)_3 \cdot 9\text{H}_2\text{O}$ (Sigma-Aldrich, 99%), $\text{Fe}(\text{NO}_4)_3 \cdot 9\text{H}_2\text{O}$ (Sigma-Aldrich, 99%), Citric acid (Alfa-Aesar, 99%), and NaH_2PO_4 (Sigma-Aldrich, 99%) were procured and directly used in the synthesis.

2.2.2. Synthesis

We synthesized five different stoichiometric compositions of $\text{Na}_3\text{Cr}_y\text{Fe}_{(2-y)}(\text{PO}_4)_3$, where $y = 0, 0.5, 1, 1.5$ and 2 , through sol-gel routes. Considering $y = 1$, we took 0.40 g of $\text{Cr}(\text{NO}_4)_3 \cdot 9\text{H}_2\text{O}$ and 0.41 g of $\text{Fe}(\text{NO}_4)_3 \cdot 9\text{H}_2\text{O}$ into a 100 mL beaker containing 60 mL DI water and kept for stirring. Followed by the addition of citric acid, the temperature raised to 60°C and stirring is

continued for 2 h. afterward NaH_2PO_4 was added into it, the colour of the solution changes into green, further stirred 2h more for homogeneous mixing. Then, the temperature was increased to 90°C for drying the samples. Thereafter, the sample was grinded with agate mortar and transferred into the ceramic boat and kept in a muffle furnace at 400°C for 6h with a heating rate $5^\circ/\text{min}$ for decompositions of nitrate and citric acid. The obtained grey product with intermediate grinding was heated in the muffle furnace at 750°C for 15h with a heating rate of $5^\circ/\text{min}$. The final product obtained was light green, similar to other compositions obtained with different temperatures. The final step was the same for $y = 0.5$ and 1.5 ; however, the final step for $y = 0$ was 750°C for 12h, the product was pink colour, and $y = 2$ was 800°C for 15h, a green colour product obtained (Table 2.1).

Table 2.1. Synthesis protocol of five different compositions

Compositions	Intermediate step			Final step		
	Temp. ($^\circ\text{C}$)	Time (hours)	Ramp rate ($^\circ\text{C}/\text{min}$)	Temp. ($^\circ\text{C}$)	Time (hours)	Ramp rate ($^\circ\text{C}/\text{min}$)
$\text{Na}_3\text{Fe}_2(\text{PO}_4)_3$	400	6	5	750	12	5
$\text{Na}_3\text{Cr}_{0.5}\text{Fe}_{1.5}(\text{PO}_4)_3$	400	6	5	750	15	5
$\text{Na}_3\text{CrFe}(\text{PO}_4)_3$	400	6	5	750	15	5
$\text{Na}_3\text{Cr}_{1.5}\text{Fe}_{0.5}\text{PO}_4)_3$	400	6	5	750	15	5

$\text{Na}_3\text{Cr}_2(\text{PO}_4)_3$	400	6	5	800	15	5
---	-----	---	---	-----	----	---

2.2.3. Characterization

Powder X-ray diffraction (PXRD) patterns of the as-synthesized products were measured using a Rigaku diffractometer (Cu $K\alpha$ ($\lambda = 1.54056 \text{ \AA}$)). Le-Bail fitting was performed on the NASICON samples to obtain cell parameters.

FESEM micrographs were obtained from the Field Emission Scanning Electron Microscopy (FESEM), Zeiss, Gemini SEM 500 with 20KV accelerating voltage. Differential scanning calorimetry (DSC) data was obtained from a METTLER TOLEDO, DSC3, STAR^e System.

All the electrochemical tests were carried out in Swagelok cells with sodium metal (Sigma-Aldrich, 99%) as the counter electrode. The working electrodes, i.e., NASICON cathodes, were prepared by ball-milling 65 wt% of active materials, 27 wt% of TIMICAL SUPER C-45 carbon (MTI), and 8 wt% of poly (vinylidene fluoride) (PVDF, MTI.) for 5 minutes. These composites were mixed with N-methyl pyrrolidine (Sigma-Aldrich, 99%) solvent and subsequently the slurries were coated on a 0.025 mm thick carbon-coated aluminium foil current collector. The electrodes were dried under vacuum at 80°C overnight and punched into discs of 10 mm diameter with active materials mass loading of $\sim 2.5 \text{ mg cm}^{-2}$. The electrolytes made of 1.0 M NaClO_4 in a mixture of propylene carbonate (PC), ethylene carbonate (EC), dimethyl carbonate (DMC.) (45:45:10 by wt%) with 2 wt% fluorinated ethylene carbonates (FEC) were used. The Swagelok cells were assembled in an argon-filled glove-box. Electrochemical measurements were performed using galvanostatic cycling with potential limitation (GCPL), in a battery cycler (BCS-805) using the voltage window 4.6-1.5V vs. Na^+/Na^0 and the current rate of C/10 as well as 1C.

2.3. Results and Discussion

The chemical composition of NASICON- $\text{Na}_3\text{Cr}_y\text{Fe}_{(2-y)}(\text{PO}_4)_3$ was estimated using ICP-OES technique and the corresponding results are displayed in table 2.2. The obtained stoichiometries are in agreement with the target compositions. The crystal structure of five different stoichiometric compositions of $\text{Na}_3\text{Cr}_y\text{Fe}_{(2-y)}(\text{PO}_4)_3$, where $y = 0, 0.5, 1, 1.5$ and 2 , was studied by PXRD. All the samples crystallize in monoclinic C2/c structure except the $\text{Na}_3\text{Cr}_2(\text{PO}_4)_3$ which adopts rhombohedral R-3c structure (Figure 2.2a). The refined lattice parameters are depicted in table 2.3. The calculated lattice parameter of $\text{Na}_3\text{Fe}_2(\text{PO}_4)_3$ and $\text{Na}_3\text{Cr}_2(\text{PO}_4)_3$ cathodes are in agreement with the literature values.

To study the phase transitions of NASICON- $\text{Na}_3\text{Cr}_y\text{Fe}_{(2-y)}(\text{PO}_4)_3$, DSC was carried out from -50 to 250 °C at a rate of 5 °/min for two heating/cooling cycles and the corresponding results are displayed in Figure 2.2 (b). The first peak of $\text{Na}_3\text{Fe}_2(\text{PO}_4)_3$ at 79.5°C is attributed to the phase transition from α to β during heat flow, where β - phase is an intermediate and α - phase is a monoclinic.¹⁹ Another small and broad peak was observed at the temperature of 130°C, which corresponds to β - phase to γ -phase transition.²⁰ The γ -phase crystallizes in rhombohedral R-3c structure. However, hysteresis was observed during cooling and a slightly shifted in temperature from 130°C to 131°C. This series of phase transitions are attributed to (dis)ordering of sodium-ions in NASICON lattice.^{20, 21} The $\text{Na}_3\text{Cr}_{0.5}\text{Fe}_{1.5}(\text{PO}_4)_3$ a single peak at 80 °C, which has a transition from α to β during heat flow. However, hysteresis was observed during cooling and a slightly shifted in temperature from 80 to 85 °C.

Table 2.2. Stoichiometric of five chemical compositions calculated and observed through ICP-OES technique.

Compositions	Na		Cr		Fe	
	Obs.	Cal.	Obs.	Cal.	Obs.	Cal.
$\text{Na}_3\text{Fe}_2(\text{PO}_4)_3$	2.37	2.99	0.0	0.0	1.88	1.99
$\text{Na}_3\text{Cr}_{0.5}\text{Fe}_{1.5}(\text{PO}_4)_3$	2.42	2.99	0.45	0.49	1.46	1.49
$\text{Na}_3\text{CrFe}(\text{PO}_4)_3$	2.44	2.99	0.97	1.0	1.0	1.0
$\text{Na}_3\text{Cr}_{1.5}\text{Fe}_{0.5}(\text{PO}_4)_3$	2.32	2.99	1.44	1.49	0.46	0.49
$\text{Na}_3\text{Cr}_2(\text{PO}_4)_3$	2.39	2.99	1.97	1.99	0.0	0.0

Fig.2.2(b) shows a single peak for $\text{Na}_3\text{CrFe}(\text{PO}_4)_3$ at 66.8°C , corresponding to the transition from α to β during heat flow. During cooling, hysteresis observed a slightly shifted temperature from 66.8°C to 71.9°C . We could not spot any clear peak for phase transition of $\text{Na}_3\text{Cr}_{1.5}\text{Fe}_{0.5}(\text{PO}_4)_3$. Finally, the $\text{Na}_3\text{Cr}_2(\text{PO}_4)_3$ show the first peak at 132.8°C , corresponding to the transition from α' to β during heat flow, where β - phase is an intermediate.²⁰ Moreover, another peak was observed at 163°C corresponding to β - phase to γ -phase transition.²² Here, γ -phase is monoclinic with a $C2/c$ space group, and α' -phase is rhombohedral with an $R-3c$ space group.²⁰ These observations show that as we have increased the stoichiometric amount of Cr in $\text{Na}_3\text{Fe}_2(\text{PO}_4)_3$ to $\text{Na}_3\text{Cr}_{0.5}\text{Fe}_{1.5}(\text{PO}_4)_3$, the peak position of phase transition from α to β remains almost the same. In contrast, the peak position of phase transition from α to β shift is observed, in case of $\text{Na}_3\text{CrFe}(\text{PO}_4)_3$ (66.8°C) as compared to $\text{Na}_3\text{Fe}_2(\text{PO}_4)_3$ (79.5°C). Moreover, $\alpha \leftrightarrow \beta$ phase transition leads to the most dynamic disorder of sodium-ions.¹⁹

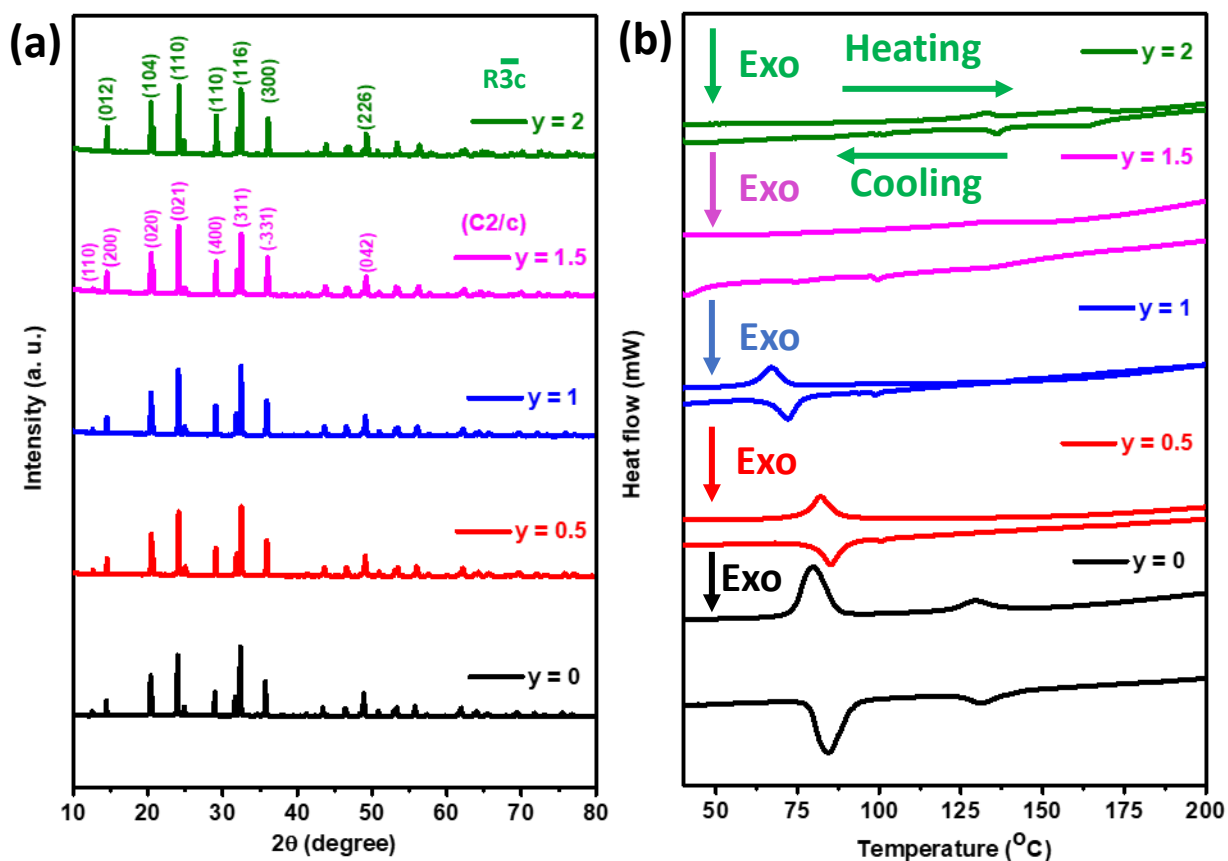


Figure 2.2. (a) XRD patterns and (b) DSC profiles of NASICON- $\text{Na}_3\text{Cr}_y\text{Fe}_{(2-y)}(\text{PO}_4)_3$.

The morphologies of NASICON- $\text{Na}_3\text{Cr}_y\text{Fe}_{(2-y)}(\text{PO}_4)_3$ cathodes were studied using SEM technique (Figure 2.3). Irrespective of Cr^{3+} substitution, all the materials exhibit irregular interconnected primary particle of ~ 200 nm.

The electrochemical Na (de)intercalation properties of the NASICON- $\text{Na}_3\text{Cr}_y\text{Fe}_{(2-y)}(\text{PO}_4)_3$ cathodes were investigated in the potential window of 4.6-1.5V vs Na^+/Na^0 at C/10 rate. Their corresponding voltage-capacity and dQ/dV profiles are depicted in Fig. 2.4. During the first charge, the $\text{Na}_3\text{Fe}_2(\text{PO}_4)_3$ cathode shows a short voltage plateau at 4 V vs Na^+/Na^0 , however, it is not reversible on the subsequent discharge. It exhibits reversible voltage plateaus at 2.5 V due to redox activity of $\text{Fe}^{3+}/\text{Fe}^{2+}$ couple with reversible capacities of ~ 78 mAh g^{-1} . The $y = 0.5$ cathode shows similar voltage-capacity and dQ/dV profiles (Figure 2.4) like the $\text{Na}_3\text{Fe}_2(\text{PO}_4)_3$ endmember. Interestingly, the $\text{Na}_3\text{FeCr}(\text{PO}_4)_3$ cathode show slightly higher first

charge capacity associated with the high voltage plateau (4.5 V) compared to those of previous members.

Table 2.3. List of the calculated lattice parameters.

System	Space group	Lattice Parameters		Volume Å³
Na₃Fe₂(PO₄)₃	C2/c	a = 15.07780 b = 8.82557 c = 8.69579	α = 90 β = 125.01428 γ = 90	947.717
Na₃Cr_{0.5}Fe_{1.5}(PO₄)₃	C2/c	a = 15.06211 b = 8.69419 c = 8.77570	α = 90 β = 125.07651 γ = 90	940.491
Na₃CrFe(PO₄)₃	C2/c	a = 15.14721 b = 8.63767 c = 8.80662	α = 90 β = 125.79242 γ = 90	934.620
Na₃Cr_{1.5}Fe_{0.5}(PO₄)₃	C2/c	a = 15.11567 b = 8.64840 c = 8.88916	α = 90 β = 125.47776 γ = 90	946.303
Na₃Cr₂(PO₄)₃	R-3c	a = 8.64729 b = 8.64729 c = 21.63510	α = 90 β = 90 γ = 120	1401.036

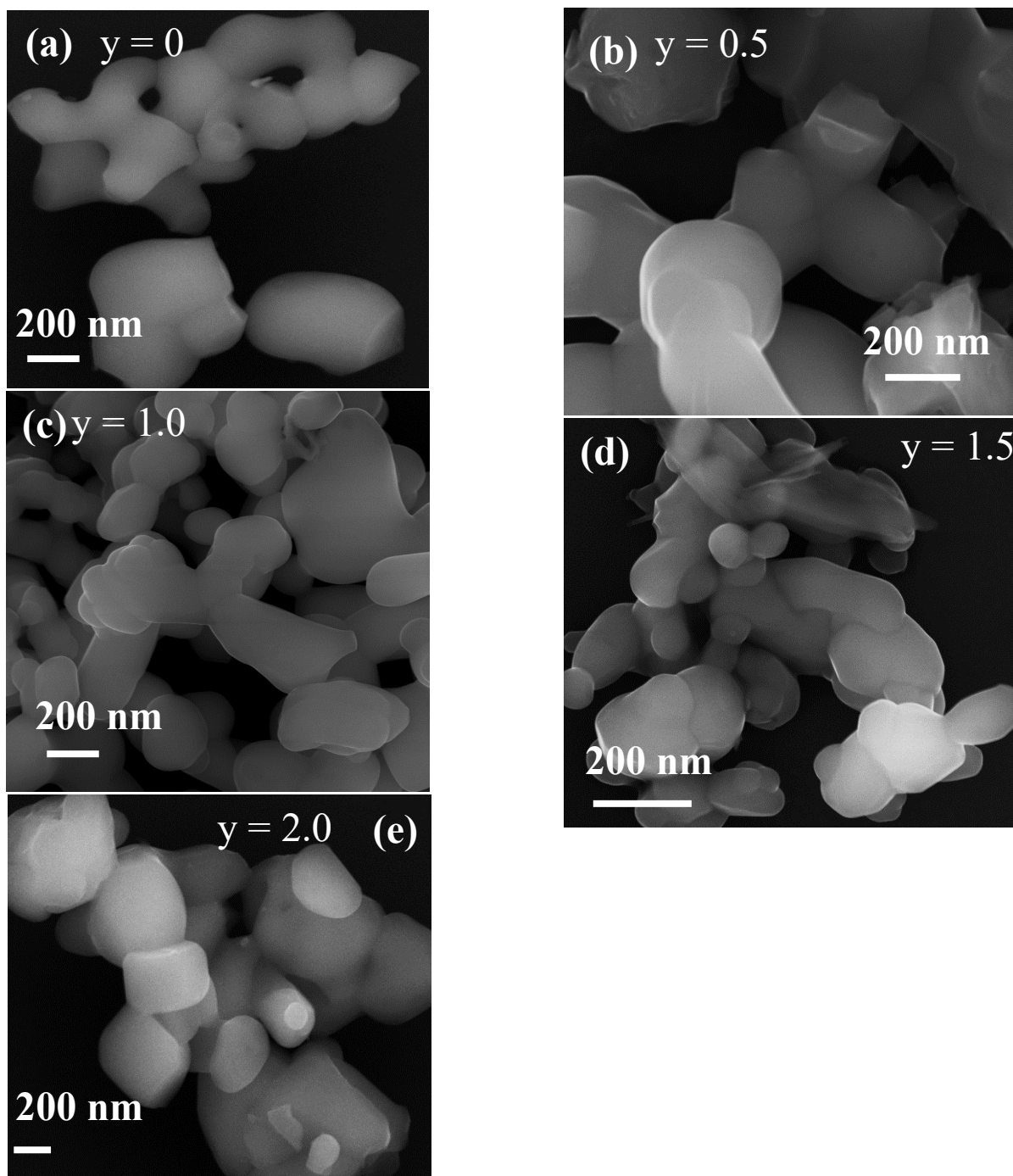


Figure 2.3. SEM images of $\text{Na}_3\text{Cr}_y\text{Fe}_{(2-y)}(\text{PO}_4)_3$.

Indeed, this high voltage plateau is noticed during the successive charging processes, but not reversible during the subsequent discharge processes. The low voltage plateau of $\text{Fe}^{3+}/\text{Fe}^{2+}$ shows reversible capacities of $\sim 100 \text{ mAh g}^{-1}$. As the Cr^{3+} ion concentration in $\text{Na}_3\text{Cr}_y\text{Fe}_{(2-y)}(\text{PO}_4)_3$ increases further, the $y = 1.5$ and 2 cathodes show featureless voltage-capacity and dQ/dV profiles with lesser capacities of $\sim 40 \text{ mAh g}^{-1}$.

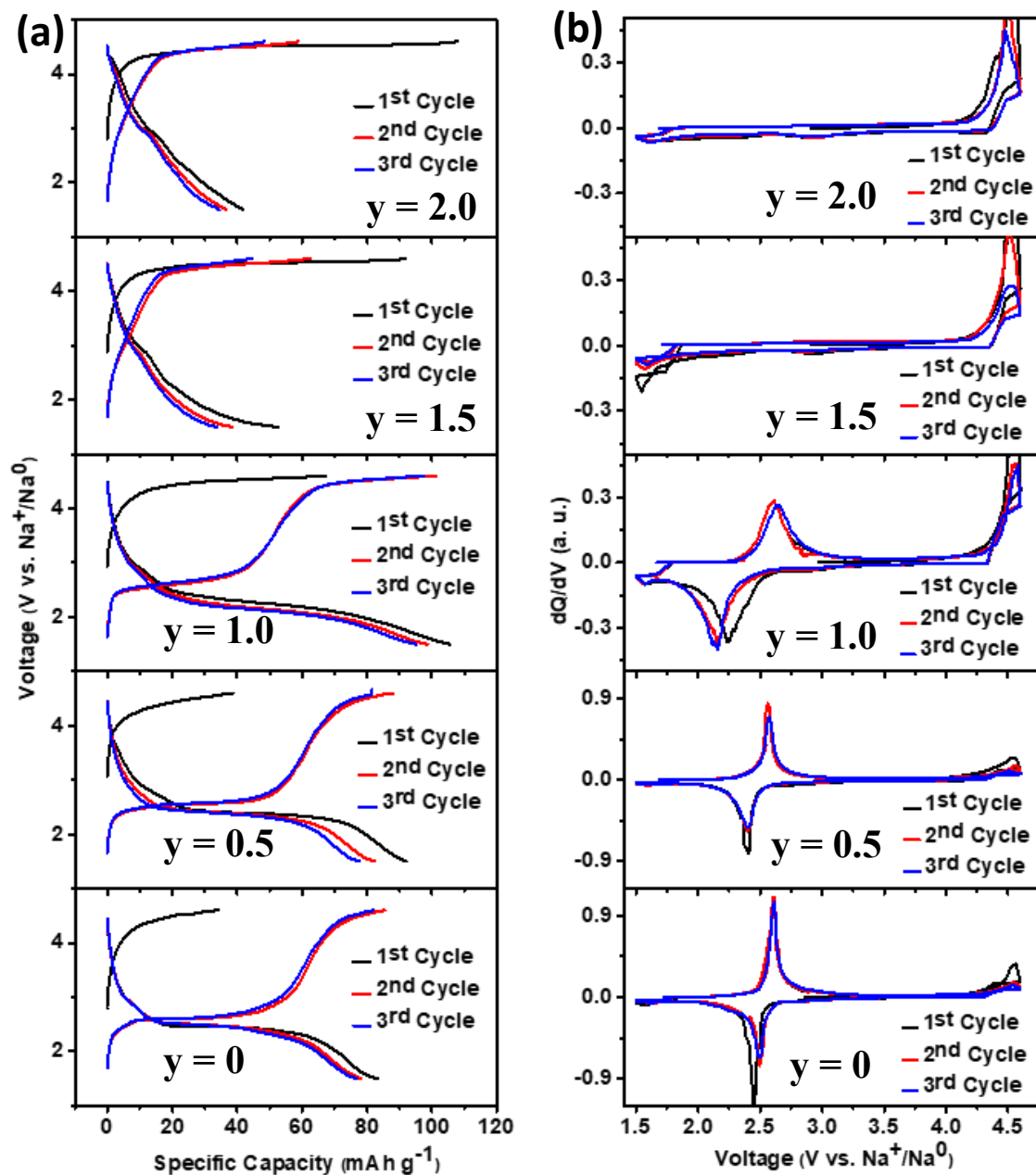


Figure 2.4. (a) voltage-capacity and (b) dQ/dV profiles of NASICON- $\text{Na}_3\text{Cr}_y\text{Fe}_{(2-y)}(\text{PO}_4)_3$ cathodes.

Further, we have attempted to improve the electrochemical performance of NASICON $\text{Na}_3\text{CrFe}(\text{PO}_4)_3$ cathode by particle downsizing using high energy ball-milling. Figure 2.5 shows the SEM images of ball-milled samples. It is clear that upon ball-milling for 30 mins the particle size is reduced below 100 nm.

Figure 2.6 shows voltage-capacity profiles and capacity retention of $\text{Na}_3\text{CrFe}(\text{PO}_4)_3$ cathode ball-milled for 30 min at 1C rate. although, the electrode delivers higher reversible capacity $\sim 100 \text{ mAh g}^{-1}$, it undergoes rapid capacity decay, reaching 24 mAh g^{-1} within 50 cycles.

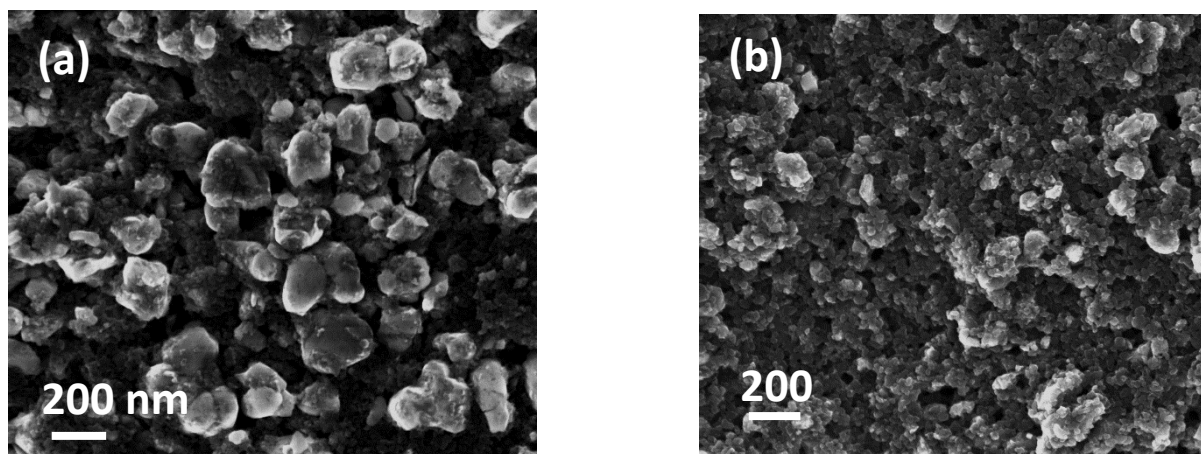


Figure 2.5. Scanning Electron Microscopy (SEM) images of $\text{Na}_3\text{CrFe}(\text{PO}_4)_3$ ball-milled for (a) 5 and (b) 30 minutes, respectively.

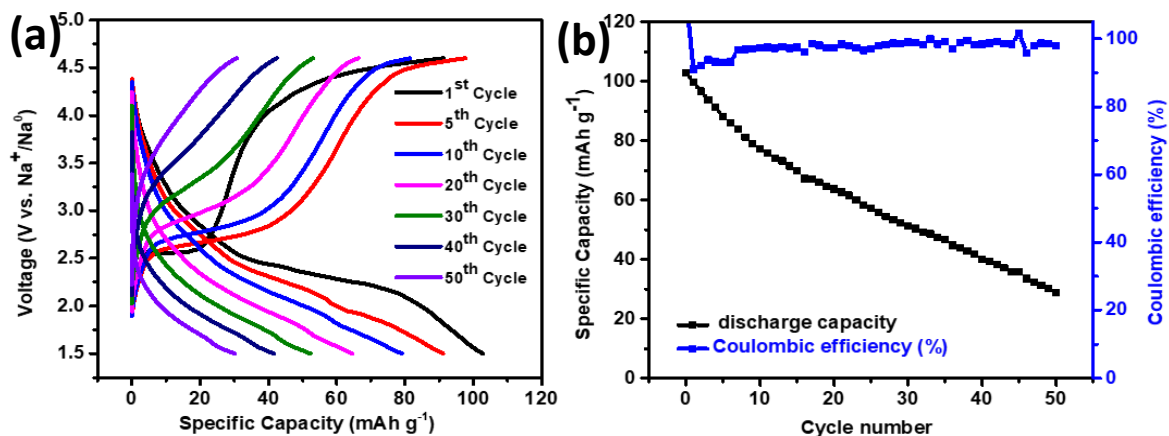


Figure 2.6. (a) Galvanostatic charge/discharge profile and (b) Cycling performance of a 30 mins ball milled $\text{Na}_3\text{CrFe}(\text{PO}_4)_3$ and with a current rate 1C.

2.4. Conclusion

In this study, we prepared a series of NASICON- $\text{Na}_3\text{Cr}_y\text{Fe}_{(2-y)}(\text{PO}_4)_3$ cathodes. Except the $\text{Na}_3\text{Cr}_2(\text{PO}_4)_3$, all the cathodes crystallize in monoclinic unit cell (C2/c space group). DSC studies reveal multiple phase transformations associated with Na order/disorder phenomena. The galvanostatic charge/discharge reveals higher reversible capacity of $\sim 100 \text{ mAh g}^{-1}$ for $\text{Na}_3\text{CrFe}(\text{PO}_4)_3$ cathode, however, it fades quickly.

2.5. References

- (1) Goodenough, J. B.; Park, K. S. The Li-Ion Rechargeable Battery: A Perspective. *J. Am. Chem. Soc.* **2013**, *135* (4), 1167–1176. <https://doi.org/10.1021/ja3091438>.
- (2) Gao, H.; Li, Y.; Park, K.; Goodenough, J. B. Sodium Extraction from NASICON-Structured $\text{Na}_3\text{MnTi}(\text{PO}_4)_3$ through Mn(III)/Mn(II) and Mn(IV)/Mn(III) Redox Couples. **2016**, No. iii, 6553–6559. <https://doi.org/10.1021/acs.chemmater.6b02096>.
- (3) Masias, A.; Marcicki, J.; Paxton, W. A. Opportunities and Challenges of Lithium Ion Batteries in Automotive Applications. *ACS Energy Lett.* **2021**, *6* (2), 621–630. <https://doi.org/10.1021/acsenergylett.0c02584>.
- (4) Dunn, B.; Kamath, H.; Tarascon, J. M. Electrical Energy Storage for the Grid: A Battery of Choices. *Science* (80-.). **2011**, *334* (6058), 928–935. <https://doi.org/10.1126/science.1212741>.
- (5) Zhang, H.; Qin, B.; Buchholz, D.; Passerini, S. High-Efficiency Sodium-Ion Battery Based on NASICON Electrodes with High Power and Long Lifespan. *ACS Appl. Energy Mater.* **2018**, *1* (11), 6425–6432. <https://doi.org/10.1021/acsaem.8b01390>.
- (6) Yang, Z.; Zhang, J.; Kintner-Meyer, M. C. W.; Lu, X.; Choi, D.; Lemmon, J. P.; Liu, J. Electrochemical Energy Storage for Green Grid. *Chem. Rev.* **2011**, *111* (5), 3577–3613. <https://doi.org/10.1021/cr100290v>.
- (7) Kundu, D.; Talaie, E.; Duffort, V.; Nazar, L. F. The Emerging Chemistry of Sodium Ion Batteries for Electrochemical Energy Storage. *Angew. Chemie - Int. Ed.* **2015**, *54* (11), 3432–3448. <https://doi.org/10.1002/anie.201410376>.
- (8) Hosaka, T.; Kubota, K.; Hameed, A. S.; Komaba, S. Research Development on K-Ion Batteries. *Chem. Rev.* **2020**, *120* (14), 6358–6466. <https://doi.org/10.1021/acs.chemrev.9b00463>.
- (9) Makhlooghiyazad, F.; Sharma, M.; Zhang, Z.; Howlett, P. C.; Forsyth, M.; Nazar, L. F. Stable High-Temperature Cycling of Na Metal Batteries on $\text{Na}_3\text{V}_2(\text{PO}_4)_3$ and $\text{Na}_2\text{FeP}_2\text{O}_7$ Cathodes in NaFSI-Rich Organic Ionic Plastic Crystal Electrolytes. *J. Phys. Chem. Lett.* **2020**, *11* (6), 2092–2100. <https://doi.org/10.1021/acs.jpcclett.0c00149>.
- (10) Hwang, J. Y.; Myung, S. T.; Sun, Y. K. Sodium-Ion Batteries: Present and Future. *Chem. Soc. Rev.* **2017**, *46* (12), 3529–3614. <https://doi.org/10.1039/c6cs00776g>.
- (11) Wang, C.; Liu, L.; Zhao, S.; Liu, Y.; Yang, Y.; Yu, H.; Lee, S.; Lee, G. H.; Kang, Y. M.; Liu, R.; Li, F.; Chen, J. Tuning Local Chemistry of P2 Layered-Oxide Cathode for High Energy and Long Cycles of Sodium-Ion Battery. *Nat. Commun.* **2021**, *12* (1), 1–9. <https://doi.org/10.1038/s41467-021-22523-3>.
- (12) Jin, T.; Li, H.; Zhu, K.; Wang, P. F.; Liu, P.; Jiao, L. Polyanion-Type Cathode Materials for Sodium-Ion Batteries. *Chem. Soc. Rev.* **2020**, *49* (8), 2342–2377. <https://doi.org/10.1039/c9cs00846b>.
- (13) Wheeler, S.; Capone, I.; Day, S.; Tang, C.; Pasta, M. Low-Potential Prussian Blue Analogues for Sodium-Ion Batteries: Manganese Hexacyanochromate. *Chem. Mater.* **2019**, *31* (7), 2619–2626. <https://doi.org/10.1021/acs.chemmater.9b00471>.

- (14) Abraham, K. M. How Comparable Are Sodium-Ion Batteries To. *ACS Energy Lett.* **2020**, 3544–3547. <https://doi.org/10.1021/acsenerylett.0c02181>.
- (15) Zhou, Y.; Shao, X.; Lam, K. H.; Zheng, Y.; Zhao, L.; Wang, K.; Zhao, J.; Chen, F.; Hou, X. Symmetric Sodium-Ion Battery Based on Dual-Electron Reactions of NASICON-Structured $\text{Na}_3\text{MnTi}(\text{PO}_4)_3$ Material. *ACS Appl. Mater. Interfaces* **2020**, *12* (27), 30328–30335. <https://doi.org/10.1021/acsam.0c05784>.
- (16) Liu, Y.; Zhou, Y.; Zhang, J.; Xia, Y.; Chen, T.; Zhang, S. Monoclinic Phase $\text{Na}_3\text{Fe}_2(\text{PO}_4)_3$: Synthesis, Structure, and Electrochemical Performance as Cathode Material in Sodium-Ion Batteries. *ACS Sustain. Chem. Eng.* **2017**, *5* (2), 1306–1314. <https://doi.org/10.1021/acssuschemeng.6b01536>.
- (17) Cao, Y.; Liu, Y.; Zhao, D.; Xia, X.; Zhang, L.; Zhang, J.; Yang, H.; Xia, Y. Highly Stable $\text{Na}_3\text{Fe}_2(\text{PO}_4)_3$ @Hard Carbon Sodium-Ion Full Cell for Low-Cost Energy Storage. *ACS Sustain. Chem. Eng.* **2020**, *8* (3), 1380–1387. <https://doi.org/10.1021/acssuschemeng.9b05098>.
- (18) Kawai, K.; Zhao, W.; Nishimura, S. I.; Yamada, A. High-Voltage $\text{Cr}^{4+}/\text{Cr}^{3+}$ Redox Couple in Polyanion Compounds. *ACS Appl. Energy Mater.* **2018**, *1* (3), 928–931. <https://doi.org/10.1021/acsaem.7b00105>.
- (19) Qiu, S.; Wu, X.; Wang, M.; Lucero, M.; Wang, Y.; Wang, J.; Yang, Z.; Xu, W.; Wang, Q.; Gu, M.; Wen, J.; Huang, Y.; Xu, Z. J.; Feng, Z. NASICON-Type $\text{Na}_3\text{Fe}_2(\text{PO}_4)_3$ as a Low-Cost and High-Rate Anode Material for Aqueous Sodium-Ion Batteries. *Nano Energy* **2019**, *64*, 103941. <https://doi.org/10.1016/J.NANOEN.2019.103941>.
- (20) d'Yvoire, F.; Pintard-Scrépel, M.; Bretey, E.; de la Rochère, M. Phase Transitions and Ionic Conduction in 3D Skeleton Phosphates $\text{A}_3\text{M}_2(\text{PO}_4)_3$: A = Li, Na, Ag, K ; M = Cr, Fe. *Solid State Ionics* **1983**, *9–10* (PART 2), 851–857. [https://doi.org/10.1016/0167-2738\(83\)90101-7](https://doi.org/10.1016/0167-2738(83)90101-7).
- (21) Kravchenko, V. V; Sigaryov, S. E. STRUCTURAL FEATURES OF THE SUPERIONIC PHASE TRANSITIONS IN $\text{Na}_3\text{Fe}_2(\text{PO}_4)_3$. *Solid state comm* **1992**, *83* (2), 149–152.
- (22) Vijayan, L.; Govindaraj, G. NASICON Materials: Structure and Electrical Properties. *Polycryst. Mater. - Theor. Pract. Asp.* **2012**, *2*, 77–106. <https://doi.org/10.5772/28967>.

